Acta Oceanol. Sin., 2020, Vol. 39, No. 3, P. 148–158
https://doi.org/10.1007/s13131-020-1533-0
http://www.hyxb.org.cn
E-mail: hyxbe@263.net

Validation and correction of sea surface salinity retrieval from SMAP

Sisi Qin[1, 2], Hui Wang[3], Jiang Zhu[4, 5], Liying Wan[3]*, Yu Zhang[3], Haoyun Wang[3, 5]

[1] National Meteorological Center, Beijing 100081, China

[2] Numerical Weather Prediction Center of China Meteorological Administration, Beijing 100081, China

[3] Key Laboratory of Research on Marine Hazards Forecasting, National Marine Environmental Forecasting Center, Beijing 100081, China

[4] International Center for Climate and Environment Sciences, Institute of Atmospheric Physics, Chinese Academy of Sciences, Beijing 100029, China

[5] University of the Chinese Academy of Sciences, Beijing 100049, China

Received 18 October 2018; accepted 12 December 2018

Abstract

In this study, sea surface salinity (SSS) Level 3 (L3) daily product derived from soil moisture active passive (SMAP) during the year 2016, was validated and compared with SSS daily products derived from soil Moisture and ocean salinity (SMOS) and in-situ measurements. Generally, the root mean square error (RMSE) of the daily SSS products is larger along the coastal areas and at high latitudes and is smaller in the tropical regions and open oceans. Comparisons between the two types of daily satellite SSS product revealed that the RMSE was higher in the daily SMOS product than in the SMAP, whereas the bias of the daily SMOS was observed to be less than that of the SMAP when compared with Argo floats data. In addition, the latitude-dependent bias and RMSE of the SMAP SSS were found to be primarily influenced by the precipitation and the sea surface temperature (SST). Then, a regression analysis method which has adopted the precipitation and SST data was used to correct the larger bias of the daily SMAP product. It was confirmed that the corrected daily SMAP product could be used for assimilation in high-resolution forecast models, due to the fact that it was demonstrated to be unbiased and much closer to the in-situ measurements than the original uncorrected SMAP product.

Key words: sea surface salinity (SSS), soil moisture active passive (SMAP), soil moisture and ocean salinity (SMOS), validation, correction

Citation: Qin Sisi, Wang Hui, Zhu Jiang, Wan Liying, Zhang Yu, Wang Haoyun. 2020. Validation and correction of sea surface salinity retrieval from SMAP. Acta Oceanologica Sinica, 39(3): 148–158, doi: 10.1007/s13131-020-1533-0

1 Introduction

The sea surface salinity (SSS) has long been known to be an important variable for monitoring and describing the state of ocean. The SSS can affect the formation of ocean water masses, as well as changes in global thermohaline circulations (Lagerloef, 2002). It can also reflect changes in precipitation, evaporation, runoff, and ice on both seasonal and interannual scales (Terray et al., 2012). The results of previous related studies have also indicated that the SSS plays an important role in the formation and extinction of ENSO (El Niño Southern Oscillation) events. Therefore, the assimilation of SSS into operational ocean forecasting systems is of great significance for improving the prediction abilities and accuracy capabilities when predicting ocean events (Hackert et al., 2014).

Data assimilation procedures, which are aimed at providing optimal initial conditions for models by combining model predictions and observations, have proven to be useful in increasing ocean forecasting abilities. Unlike other ocean parameters, such as the sea surface temperature (SST) and Sea Level Anomalies (SLA), as well as ocean subsurface temperature and salinity profiles, which have already been assimilated into existing operational global ocean forecasting systems, the SSS has not yet been assimilated due to limited data coverage. However, this situation will be changed with using of satellite SSS products. Since the observational data used in operational ocean forecasting assimilation systems are daily products, this study only focused on the available daily satellite SSS products.

At the current time, only three satellites exist which have the ability to retrieve SSS. These include the soil moisture and ocean salinity (SMOS) satellite (Font et al., 2001); Aquarius/SAC-D satellite (Lagerloef et al., 2008); and the soil moisture active passive (SMAP) satellite (Yueh and Chaubell, 2012), which were launched in 2009 by the European Space Agency (ESA); and in 2011 and 2015 by the National Aeronautics and Space Administration (NASA), respectively. After a few years into their missions, the SMOS (2010 to –); Aquarius (2011 to 2015); and SMAP (2015 to –) have been able to provide global SSS maps with multiple spatial and temporal resolution for several years. The satellite SSS measurements are based on L-band microwave sensitivity to water salinity, which is influenced by surface roughness, incidence angles, and polarization. They are also known to be sensitive to land and ice contamination, galactic radiation, Faraday rotations,

Foundation item: The National Key Research and Development Program of China under contract Nos 2016YFC1401409 and 2016YFC1401704; the National Natural Science Foundation of China under contract Nos 41506031 and 41606029.
*Corresponding author, E-mail: liying.wan@nmefc.cn

solar radiation, radio frequency interference (RFI), and the degree of white capping and foam coverage. Therefore, the accuracy of satellite SSS is suggested to be less than the *in-situ* measurements (Reul et al., 2007; Banks et al., 2012; Tang et al., 2014; Yueh et al., 2014; Martin, 2016; Boutin et al., 2018). So far, only a few studies have been performed regarding the validations of the SMOS, Aquarius, and SMAP satellite SSS products using Argo floats, moored-buoy data, ship-based thermo-salinograph (TSG) data, and operational ocean model outputs (Banks et al., 2012; Boutin et al, 2012, 2018; Abe and Ebuchi, 2014; Ebuchi and Abe, 2014; Ratheesh et al., 2014; Reagan et al., 2014; Drucker and Riser, 2014; Tang et al., 2014, 2017; Lee, 2016; Martin, 2016; Garcia-Eidell et al., 2017). Generally, the large-scale SSS patterns, and the variabilities in the satellite SSS products have been in agreement with the *in-situ* measurements and the operational model outputs in the open ocean. The SSS errors between the satellites and the *in-situ* measurements in coastal and high-latitude regions have been found to be larger than in the open ocean and at middle latitudes. However, the SSS bias in the coastal regions have decreased with the newly released SMOS Level 3 (L3) products due to improvements in the algorithms used in the retrieval processes (Boutin et al., 2018). Moreover, the satellite SSS can also be used to study the mesoscale phenomena in those regions (Kolodziejczyk et al., 2015).

In this paper, only the SMOS and SMAP products were discussed, since the Aquarius satellite had ended its mission in 2015. The SMOS and SMAP satellites are sun-synchronous polar orbit satellites, with exact repeating cycles of 23 days (global coverage of SMOS: every 3 to 5 days) and eight days, respectively. Therefore, the temporal resolution of the majority of the satellite L3 SSS products is monthly, ten days, or four days. The previous validation studies had mainly focused on the timescales of products larger than seven days. The Centre Aval de Traitement des Donnees SMOS (CATDS) provides two types SMOS L3 daily products with a rectangular grid (0.5°), and an EASE2 (Equal-Area Scalable Earth 2) grid (approximately 25 km), respectively. Meanwhile, the Jet Propulsion Laboratory (JPL) and Remote Sensing Systems (RSS) both provide SMAP L3 daily product with a resolution of 0.25°. It should be noted that the SMAP L3 daily products were created by an 8-day running average within ± 3.5 days, since the SMAP had an exact 8-day repeating cycle. The SMAP is equipped with classical L-band radiometers, and also has the benefits of an improved RFI-protected onboard processer. It has been found that its performances had exceeded the SMOS in the coastal regions (Boutin et al., 2018). Also, the SMAP L3 daily product has a higher resolution and coverage than the SMOS.

In this paper, the daily SMAP and SMOS products was validated with *in-situ* measurements, and the SMAP product was further bias corrected using the reanalysis data. The satellite SSS products, *in-situ* profiles, and global reanalysis data are described in detail in Section 2. The validations of the daily satellite products are presented in Section 3. The daily SMAP SSS product was bias corrected and evaluated, as shown in Section 4. Finally, in Section 5, this study's discussion and conclusions are provided.

2 Data

2.1 *SSS satellite data*

2.1.1 *SMAP data*

The primary goal of the SMAP mission is the retrieval of measurements over land. However, the L-band microwave instrument enables the SMAP to retrieve SSS over ocean. This satellite was launched in January of 2015 by NASA and began providing data in April of 2015. The SMAP L3 daily SSS product used in this study was obtained from Remote Sensing Systems (ftp://ftp.remss.com/smap) SMAP SSS V2.0 products (Meissner and Wentz, 2016). The L3 product is gridded by L2c salinity values, and the SMAP L2 data is derived from the SMAP L1B data files by following the basic steps of the Aquarius L2 V5.0 salinity retrieval algorithm (Meissner et al., 2018), with some improvements added. Due to the uncertain accuracy of the initial satellite measurements, this study used the SMAP L3 daily product (Fig. 1a) during 2016 to estimate the SSS retrieval errors.

2.1.2 *SMOS data*

The objectives of the SMOS mission include providing soil moisture and ocean salinity mapping information. This satellite was launched on November 2, 2009. Its Level 1 and 2 products are provided by an SMOS mission center which was designed by and is located in the European Space Agency (ESA)/Villafranca Center, Spain. Meanwhile, the Level 3 and 4 products are developed at various centers. In this work, the data product is extracted from the Ocean Salinity Expertise Center (CECOS) of the CNES-IFREMER Centre Aval de Traitemenent des Donnees SMOS (CATDS), which is located at IFREMER, Plouzane, France (http://www.catds.fr). The CATDS provides various SSS L3 products which are based on different retrieval algorithms. The full descriptions of these algorithms are available on the following website: http://www.catds.fr/Resources/Documentation. The CATDS also provides SSS L3 daily products which are processed by the CATDS Ifremer Expertise Center (CEC) and Data Production Center (CPDC). Among these, the CEC daily product is combined from ascending and descending passes for the considered days on rectangular grids $\left(\frac{1}{2}\right)^{\circ}$, while the CPDC daily products are products without composite passes on irregular grids. In the present study, the CEC L3 daily product for 2016 was utilized, as detailed in Fig. 1b.

2.2 *In-situ measurements*

2.2.1 *Argo floats*

The Argo Project provides global *in-situ* salinity and temperature profiles for the top 2 000 m of ocean via 3 000 free-drifting profiling floats (Gould et al., 2004). The daily floats data used in this study were extracted from the Coriolis Argo Global Data Assembly Centre (ftp://ftp.ifremer.fr/ifremer/argo/). Although the Argo program is not designed to measure the salinity of the top few centimeters of the ocean (the satellite measures SSS in the top 1 to 2 cm), considering the coverage of the Argo profiles and the small effects of the vertical salinity structure on the errors of the large-scale evaluations, the shallowest salinity data from the Argo floats are currently used to estimate the SSS errors (Abe and Ebuchi, 2014; Drucker and Riser, 2014; Reagan et al., 2014; Tang et al., 2014; Lu et al., 2016; Martin, 2016). In this study, the Argo floats data were filtered prior to use, in order to select only the profiles for which the following applied: (1) the Argo floats may be either delayed or in real-time with corrections; (2) the quality flag markers indicate good results; (3) the first measured layer is less than 6 m in depth; and (4) at least two layers which are less than 6 m in depth are present. In addition, all chosen profiles were linearly interpolated to the top ten meters, and only a 6 m layer was chosen to represent the SSS. The global SSS map of the

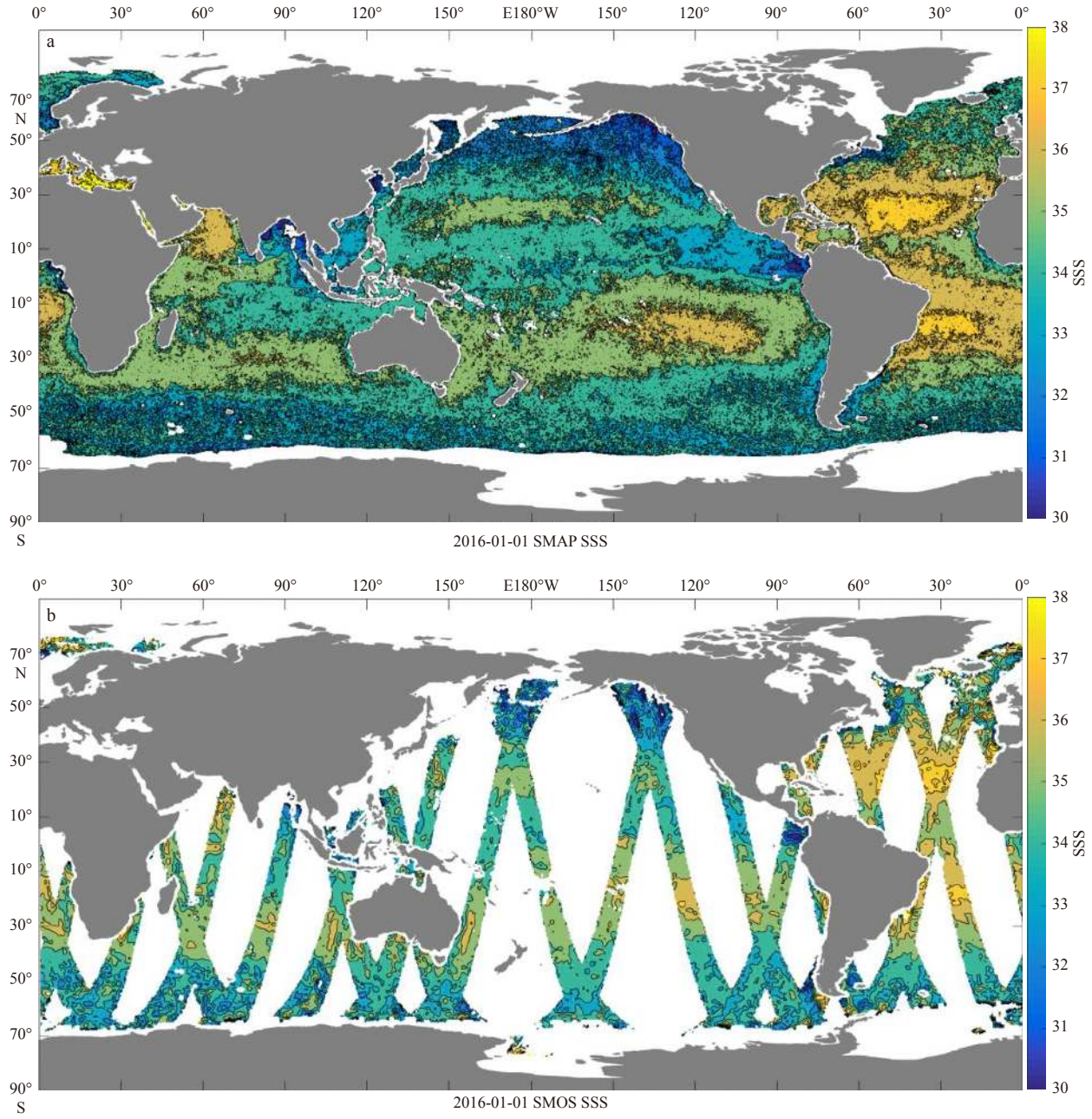

Fig. 1. Global SSS map extracted from the SMAP L3 daily product (a) and the SMOS L3 daily product (b) for 1 January 2016.

chosen daily Argo profiles for January 1, 2016 is shown in Fig. 2.

2.2.2 *Moored buoys*

The time series of the daily near-surface salinity data were obtained from a global tropical moored-buoy array, which include the Tropical Atmosphere Ocean and Triangle Trans-Ocean Buoy Network (TAO/TRITON) array in the Pacific, the Pilot Research Moored Array in the Tropical Atlantic (PIRATA), and the Research Moored Array for the Africa-Asian-Australian Monsoon Analysis and Prediction (RAMA) system in the Indian Ocean (McPhaden, 1995; Servain et al., 1998; McPhaden et al., 2009). These data were obtained from the Global Tropical Moored Buoy Array (GTMBA) office of the National Oceanic and Atmospheric Administration (NOAA), and the Pacific Marine Environmental Laboratory (PMEL). The accuracy of the moored-buoy data has approached 0.02 measured at 1 m, and were used in this study as a supplement for the Argo floats data. Also, only the data with the highest or default quality control values during 2016 were used in the current study.

2.3 *Global reanalysis data*

As mentioned in the previous related studies (Tang et al., 2017; Boutin et al., 2018), the sea surface roughness caused by wind and rain conditions, is known to significantly influence the accuracy of the SSS products. Therefore, in order to correct the bias of the SMAP SSS L3 daily product, the monthly mean precipitation, SST, and wind speed data at 10 m which were obtained from the ERA-Interim global analysis datasets (Berrisford et al., 2011) during 2016 were used in this study. The spatial resolution of the reanalysis data is 0.25°, which is the same as that of the

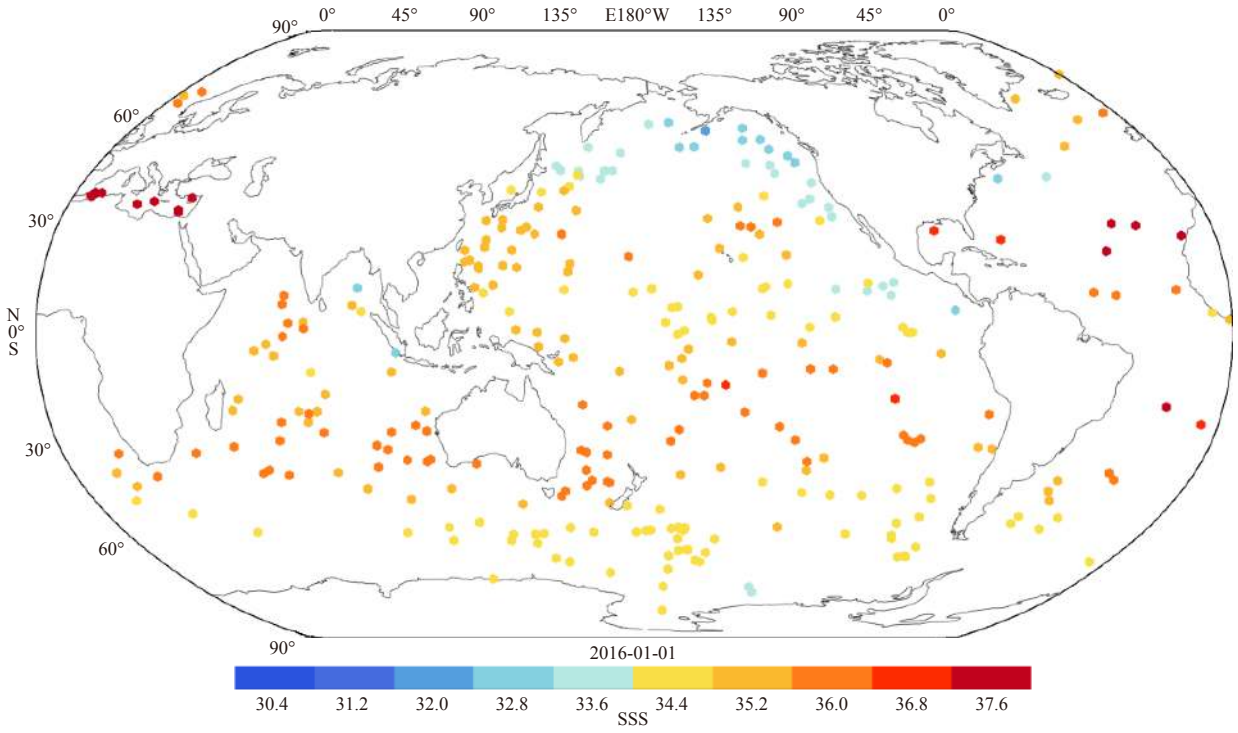

Fig. 2. Global SSS map extracted from Argo profiles for January 1, 2016.

SMAP daily product.

3 Comparison between the satellite and *in-situ* measurements

This study's comparison results between the SMAP and SMOS L3 daily product validated against the daily Argo profiles and moored-buoy data are presented in the following section. Tang et al. (2017) have previously validated SMAP L3 daily and monthly products obtained from JPL with *in-situ* salinity, and have confirmed that the SMAP SSS had the ability to accurately reflect the variabilities of the SSS on weekly and monthly timescales. In contrast with the method used by Tang et al. (2017), the daily *in-situ* SSS measurements were not averaged within eight-day periods, and only daily products were used in this study to detect the daily SSS errors of the satellite products.

3.1 *Satellite SSS and Argo floats data*

Considering the fact that numbers of the daily Argo floats are lower in some regions, and they are inconsistent in the spatial resolution between the Argo floats and the satellites, two methods were taken in order to detect the differences between Argo floats and the satellites. First, the scatter plots were obtained by comparing satellite data with the nearest Argo floats within a distance of 0.5°, since the satellites represent the spatial average of the instantaneous measurements in a footprint of approximately 40 km. Second, the global distribution maps of the SSS errors were obtained by comparing the bias and RMSE between the satellite and the nearest Argo floats within a distance of 2.5°, since the Argo floats were sparsely distributed and the SSS has small changes in the distance of 2.5°.

Figure 3 details the scatter plots of the SMOS and SMAP daily SSS versus the Argo floats data from January 1, 2016 to December 31, 2016. The numbers of the collocated data had differed, the numbers of SMAP dataset (n=95 713) have a higher spatial resolution, and was therefore larger than that of the SMOS (n=42 799). As shown in Fig. 3, both the SMOS and SMAP daily SSS data have agreed with the Argo data. The results of this study's comparison of the two scatter plots revealed that the SMAP had more high-salinity data between 38 and 40 than the SMOS. These differences were assumed to have probably been caused by the higher spatial resolution of the SMAP data, which were enabled the capture of a greater number of salinity signals. In addition, the SMOS SSS data displayed more deviations from the Argo data, with a larger RMSE (0.723) than that of the SMAP data (0.491). These results may due to the 8-day averaged process used in the SMAP daily product retrieval procedure.

As shown in Fig. 4, the distributions of the bias and RMSE for the SMOS and SMAP data versus the Argo data were observed to be inconsistent in the global ocean areas. It can be seen in the figure that the RMSE for the SMOS and SMAP products had similar distributions. Generally, both were lower in the subtropical regions and open ocean areas and were larger near the coastal areas and in the high-latitude ocean regions. Comparisons between the RMSE for the SMOS and SMAP products revealed that that the former was larger. However, the distribution of the bias of the two products was found to differ. For example, the SMAP had displayed a larger bias in the western Pacific Ocean warm pool, while the SMOS had a larger bias in the eastern Pacific cold tongue. These observed differences were assumed to have probably resulted from high precipitation and strong wind conditions, respectively. The bias of both products was found to be larger along the coastal and high-latitude regions, which were similar with the distribution patterns obtained from the monthly product data. The large coastal bias was assumed to have probably resulted from influences of RFI and land contamination.

In order to further evaluate the SSS error distributions, this study divided the ocean into five areas as follows: Indian Ocean (30°N–40°S, 40°–100°E); Pacific (60°N–40°S, 110°E–90°W); Atlantic (60°N–40°S, 70°W–20°E); west coast of the North Pacific

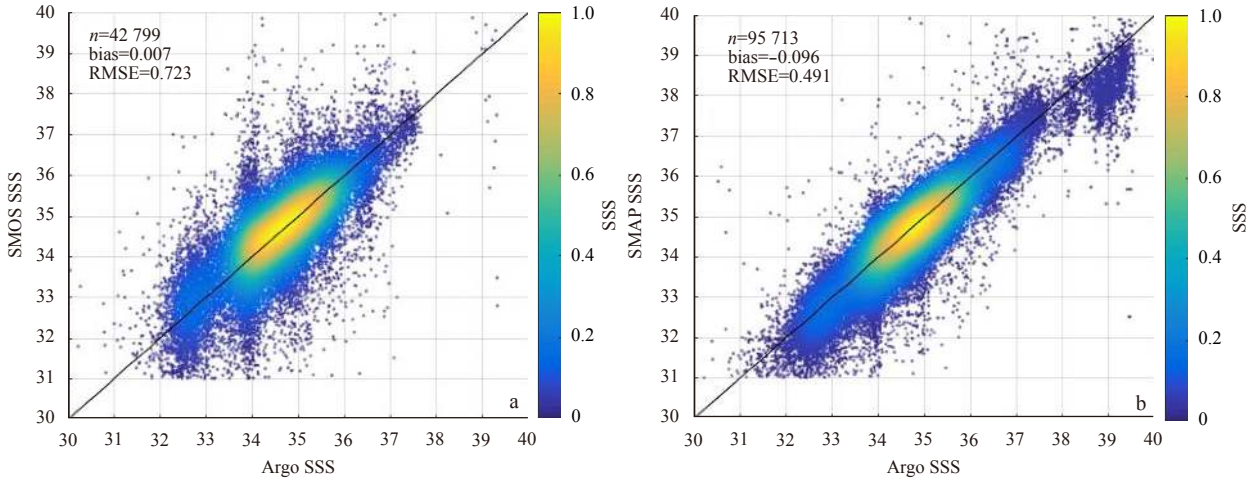

Fig. 3. Scatter plots of the SMOS (a) and SMAP (b) daily SSS data versus the Argo floats data SSS from January 1, 2016 to December 31, 2016.

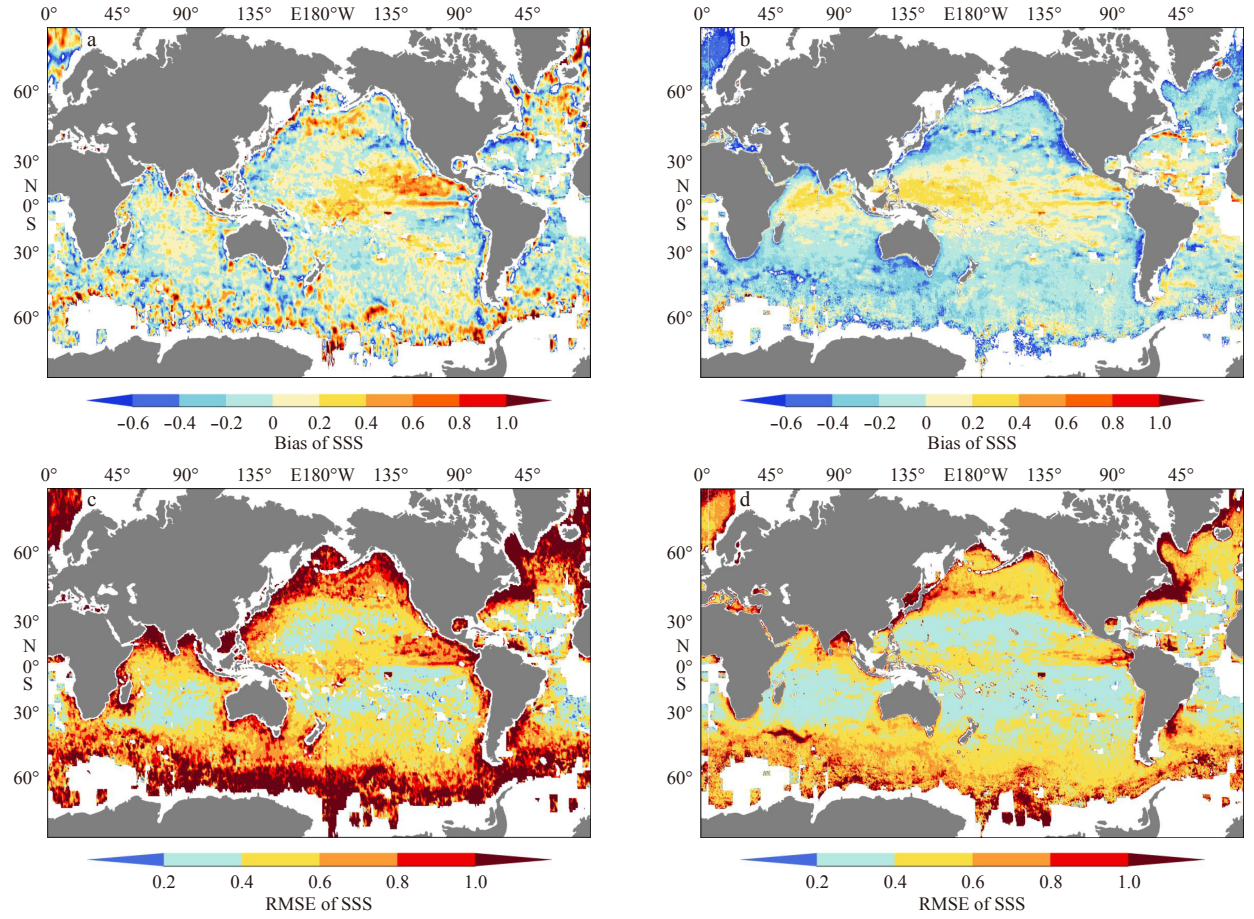

Fig. 4. Global distribution of the: bias of SSS (a, b); and RMSE of SSS (c, d) between the SMOS (a, c) and SMAP (b, d) versus the Argo floats data during the year 2016

(20°–50°N, 125°–145°E) and the open ocean areas of the Pacific (0°–40°N, 165°E–150°W). The last two areas were referred to in this study as the WCNP and OPPA, and were used to assess the errors between the coastal and open ocean regions. Table 1 lists the bias and RMSE for SMOS and SMAP data versus the Argo floats data within 0.5°, which were calculated for the five aforementioned areas. It was found that the bias of the SMOS was smaller than that of the SMAP. Meanwhile, the RMSE of the SMAP was observed to be smaller than that of the SMOS. The SMAP SSS have generally displayed a negative bias, while the sign of the SMOS SSS bias have been found to vary. Comparisons between the errors in the WCNP and OPPA indicated that the bi-

Table 1. Bias and RMSE between the satellite and Argo SSS

	SMOS (daily)		SMAP (daily)	
	Bias	RMSE	Bias	RMSE
Global	0.007	0.723	−0.096	0.556
Indian Ocean	−0.007	0.702	−0.065	0.432
Pacific	0.043	0.612	−0.050	0.443
Atlantic	−0.217	0.886	−0.137	0.582
WCNP	−0.206	0.864	−0.364	0.672
OPPA	0.039	0.454	0.039	0.372

as and RMSE in the WCNP were twice as large as those in the OPPA. The absolute bias and RMSE values for the WCNP had reached 0.3 and 0.8 , respectively. These findings suggested that quality control measures were required when using satellite SSS in the coastal regions. However, the satellite SSS was found to be of good quality in the open ocean areas, with the average daily bias and RMSE determined to be 0.039 and 0.372 , respectively. In this study, a comparison of the three largest oceans (Indian, Pacific, and Atlantic) showed that the errors between the Indian Ocean and Pacific were nearly the same, while the errors in the Atlantic had differed. The bias and RMSE of the Atlantic have nearly reached the values observed in the coastal areas, which may have been caused by the sparsity and locations of the Argo floats in the Atlantic (Fig. 2).

For the purpose of further analyzing the large errors in the Atlantic and the error distributions of the three largest oceans, the number of matched Argo floats (n), and the bias and RMSE of the SMOS and SMAP versus the Argo data, were calculated in each latitude band (10°) for the Indian Ocean, Pacific, and Atlantic, respectively, as detailed in Fig. 5. Then, the monthly mean (based on the daily mean) precipitation, wind speed at 10 m, and SST were used in this study's correlation analysis process in order to determine the contributions to the latitude-dependent error distributions of the SSS. The values for the n, bias, and RMSE were scaled in order to show within the same plot. To clarify, the values for the N and bias were scaled using different coefficients for each of the oceans, whereas the RMSE was scaled using one coefficient. Figure 5a and d show that the RMSE for each latitude band of the SMAP was less than that of the SMOS in the Indian Ocean. However, the bias showed the opposite trend. It was observed that the RMSE was lower in the tropical regions and increased with latitude. In regard to the SMOS, the minimum value occurred in the 30°S to 40°S band (0.382), while the minimum value of the SMAP occurred between 10°S and 30°S (0.328).

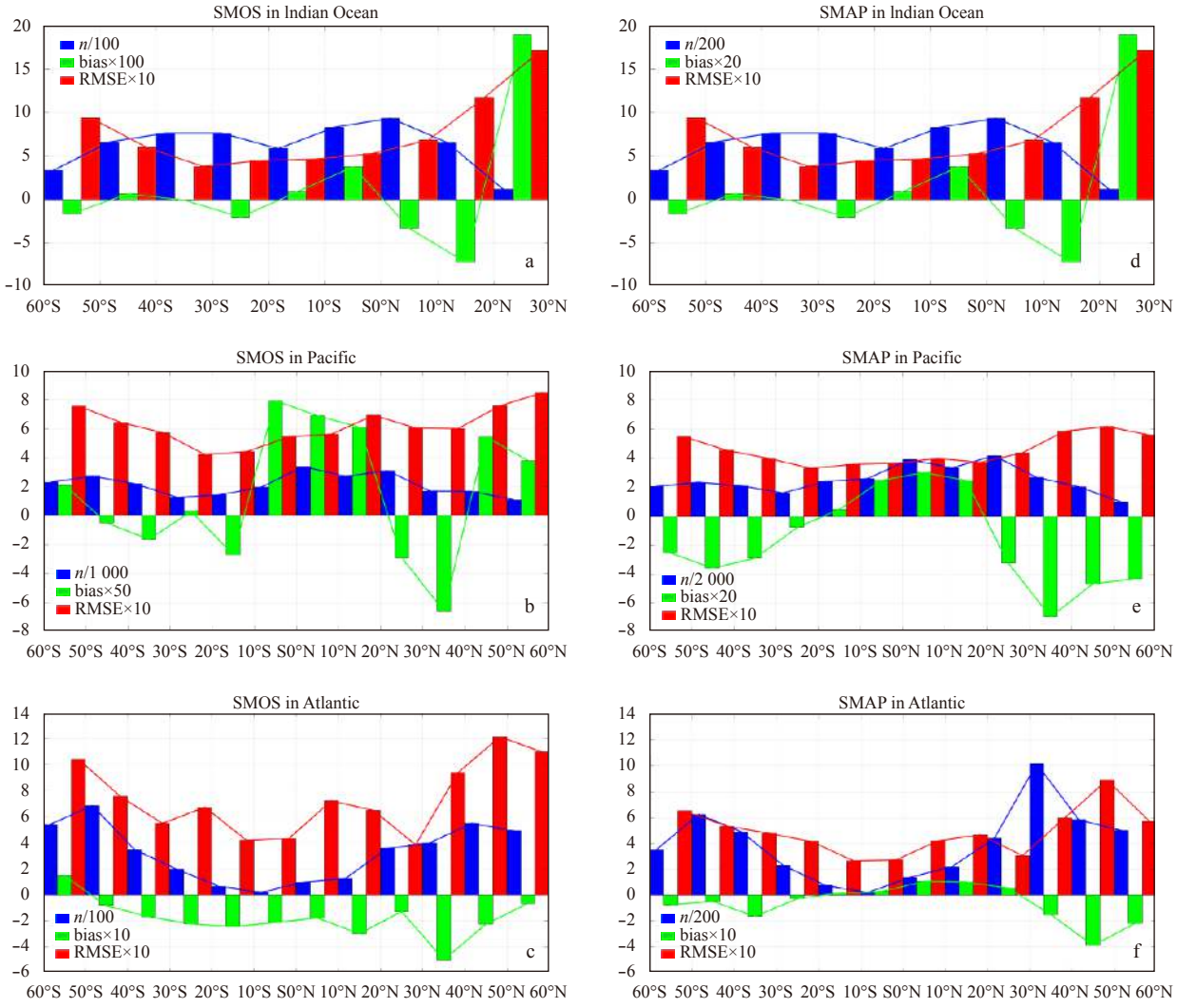

Fig. 5. Distributions of the number of matched Argo floats (n; blue); bias (green); and RMSE (red) between the daily satellite and Argo floats SSS in each latitude band of the Indian Ocean (a, d), Pacific (b, e) and Atlantic (c, f).

The bias of the SMOS displayed small absolute values, which were lower than 0.04 and reached 0.000 5 in the 30°S to 40°S band. However, it was found that the bias of the SMAP, which displayed larger bias values, followed the same trend as the precipitation (correlation coefficient of 0.82). In addition, comparisons between the *n*, bias, and RMSE revealed that the number of matched Argo floats did not have any significant influences on the bias or the RMSE. The bias and RMSE were found to be mainly dependent on the locations of the Argo floats. As shown in Figs 5b and c, the Pacific had the highest number of matched Argos floats. In addition, the latitude-dependent distributions of the *n* and RMSE for the SMOS and SMAP were observed to be nearly the same. Both distributions displayed valleys (0.329 for the SMAP and 0.421 for the SMOS) in the 20°S to 30°S band, and peak values occurred at the high latitudes. A large RMSE also existed in the 10°N to 20°N band for the SMOS. Meanwhile, the largest RMSE for the SMAP occurred in the 0° to 10°N band. It was observed that unlike the SMOS, the bias of the SMAP also showed a precipitation trend (correlation coefficient of 0.81). Furthermore, the latitude-dependent RMSE of the SSS in the Pacific was found to be primarily influenced by the SST (correlation coefficient of –0.79). The Atlantic was confirmed to have the lowest N, with low values occurring particularly between 20°S and 20°N (Figs. 5c and f), which explained why it had displayed the largest errors. In the Atlantic, the SMAP had a lower RMSE than the SMOS, as was also the case for the Indian Ocean and Pacific. The RMSE values of both the SMOS and SMAP displayed valleys in the 20°S to 0° and 20°N to 30°N bands, and peak values occurred at the high latitudes. However, unlike the other two oceans, the bias of the SMAP in the Atlantic was found to be lower than that of the SMOS, while the RMSE of the SMAP remained lower than that of the SMOS. Correlation analysis indicated that the latitude-dependent RMSE of the SSS in the Atlantic was also primarily influenced by the SST (correlation coefficient of –0.66).

In summary, comparisons between the daily SSS products of SMAP and SMOS versus the Argo floats data showed that the bias of the SMOS was lower than that of the SMAP. Meanwhile, the RMSE showed the opposite trend. The RMSE and bias were found to vary in the global oceans, with larger values along the coastal and high latitude regions, and lower values in the open ocean and tropical regions. These were found to be primarily caused by the influences of the SST and RFI on the SSS inversions. Moreover, the latitude-dependent RMSE of the SMAP was primarily influenced by the SST. It was observed that lower RMSE values consistently occurred with higher SST, lower wind speed, and weaker precipitation conditions. The bias of the SMAP was confirmed to be highly related to the precipitation conditions, which could be further used to correct the bias of the SMAP.

3.2 *Satellite SSS and moored-buoy data*

The daily measured SSS at a 1 m depth from the RAMA, TAO, and PIRATA buoy arrays during 2016 were used in this study. Since the RAMA, TAO, and PIRATA are moored-buoy arrays located in the tropical Indian Ocean, Pacific, and Atlantic, respectively, comparisons with the satellite SSS allowed for the performances of the satellite SSS products in the three largest oceans to be further explored. As shown in Fig. 6, despite the fact that they displayed different biases and RMSE values, the distribution patterns and high-density areas of the SMOS and SMAP products versus the buoy array data were obviously similar. It was observed that unlike the previous comparisons with the Argo data (Fig. 3), both the bias and RMSE of the SMAP (0.09 to 0.14 ; 0.26 to 0.37, respectively) were lower than those of the SMOS (–0.2 to 0.13 ; 0.56 to 0.57, respectively). Moreover, the comparison results of the scatter plots for the various oceans showed that the daily SMAP products had lower RMSE (0.255) in the Atlantic.

The time series of the SSS data at three buoys located in the Indian Ocean, Pacific, and Atlantic are shown in Fig. 7. It can be seen in the figure that the SMAP daily product have similar variabilities as those of the moored buoys in the three largest oceans, with correlation coefficients of approximately 0.8. In addition, the bias and RMSE values were calculated for the satellite SSS L3 daily products and the buoy SSS data. It was observed that at all three locations, the RMSE was always the largest for the SMOS daily data, whereas the SMAP daily data displayed a good agreement with the buoy data, with biases of approximately 0.1, and RMSE values lower than 0.3, as detailed in Table 2.

In conclusion, comparisons of the daily SMOS and SMAP SSS versus moored-buoy array data indicated that the RMSE of the daily SMAP product was lower than that of the daily SMOS product.

4 SMAP SSS data corrections

From the results presented in Section 3, the daily SMAP product has lower RMSE, but larger bias. Therefore, the SMAP product was bias-corrected before been assimilated into the ocean forecasting models. Then, based on the monthly precipitation and SST data obtained from the ERA-Interim data, the bias of the daily SMAP product was corrected using the following equation:

$$\text{bias}_{\text{lat}} = a + b \times \text{precipitation} + c \times \text{SST}, \tag{1}$$

where the coefficients *a*, *b*, and *c* can be obtained using regression analysis.

Correlation analysis (Section 3.1) indicated that the latitude-dependent bias and RMSE of the SMAP daily product was highly dependent on the precipitation and SST conditions. Then, by considering the monthly-varying latitudinal biases of the SMAP in the Indian Ocean, Pacific, and Atlantic, respectively, the bias-correction process used in this study could be described as follows: (1) using the daily Argo floats data and SMAP product in the Indian Ocean, Pacific, and Atlantic, respectively, to calculate the monthly bias and averaged daily bias of each month in each ocean for each of the ten latitudes (similar to Fig. 5, with the exception that Fig. 5 displays the yearly averaged monthly bias); (2) utilizing the monthly SST, precipitation, and bias results in each of the ocean of the ten latitudes to obtain the coefficients in the above equation (*a*, *b*, and *c*) for each month of each ocean, respectively; (3) using the coefficients obtained in Step 2, and the monthly precipitation and SST data, the SMAP bias on each grid in each month was calculated; (4) The original daily SMAP product was then bias-corrected by subtracting the biases obtained in Step 3.

Comparisons between the corrected (unbiased) and uncorrected (biased) SSS products in the Indian Ocean and Pacific are shown in Fig. 8. The bias between the daily SMAP and Argo floats data in the Indian Ocean and Pacific had decreased from –0.074 to 0.036, and –0.064 to 0.008, respectively, when the corrections were applied. The RMSE between the daily SMAP and Argo floats data in the Indian Ocean and Pacific had decreased from 0.443 to 0.435, and 0.449 to 0.439, respectively. The correction process was not performed in the Atlantic due to the fewer available daily Argo floats, especially in the lower latitudes. As shown in Fig. 8,

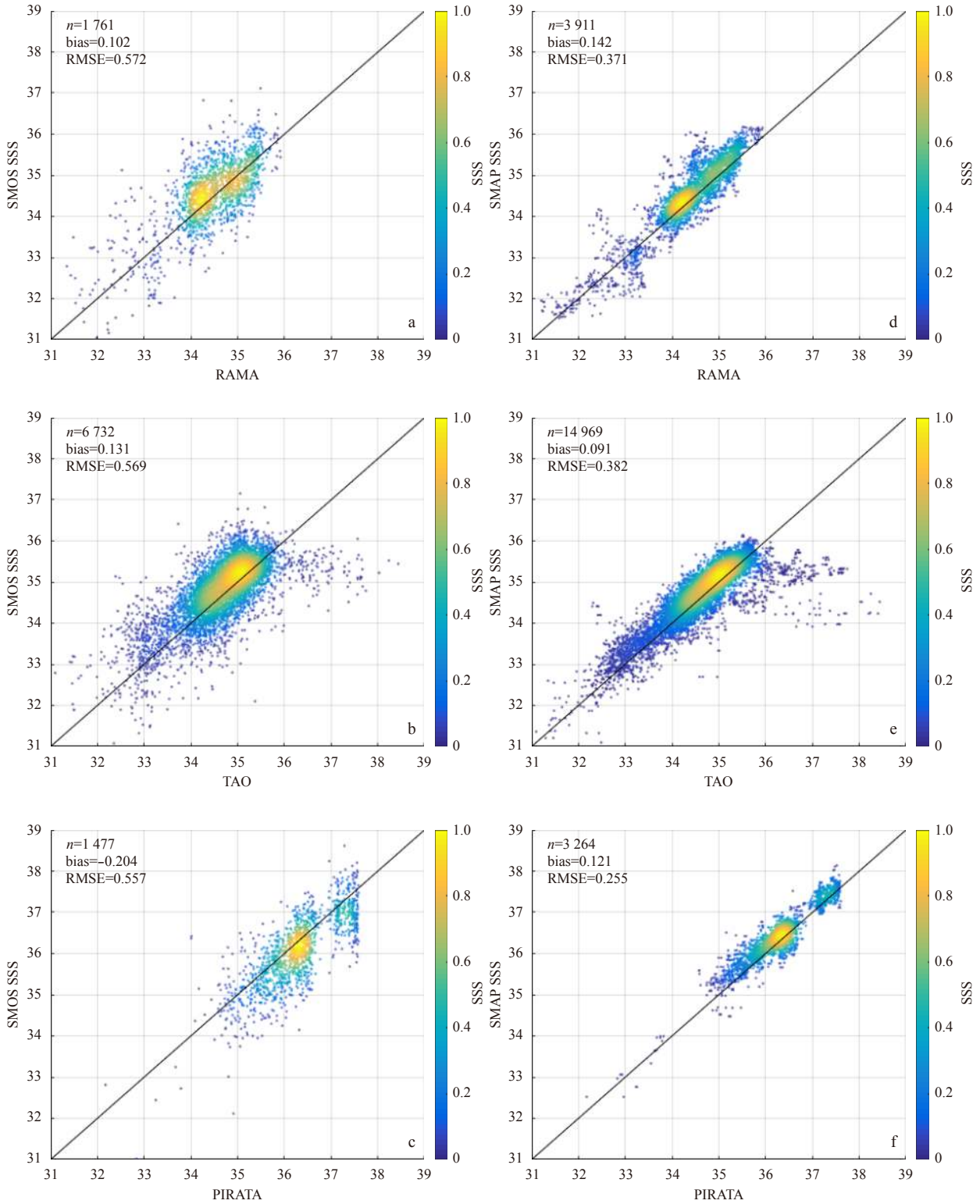

Fig. 6. Scatter plots of the SMOS and SMAP daily SSS versus the moored buoy data, from January 1, 2016 to December 31, 2016. a. SMOS versus RAMA, b. SMOS versus TAO, c. SMOS versus PIRATA, d. SMAP versus RAMA, e. SMAP versus TAO, and f. SMAP versus PIRATA.

the SSS products were more concentrated following the corrections, while the outliers were observed to be less changed. It was believed that these results likely meant that the outliers in the SMAP SSS products were mainly located near coastal areas, and required further corrects using a land-sea contamination correction process. The biased and unbiased SMAP products were also compared with the TAO data at 0°, 156°E (Fig. 9), which was observed to have a larger bias and RMSE than the other buoys, as described in Section 3.2. The bias between the SMAP product and TAO was observed to have decreased from 0.17 to –0.034,

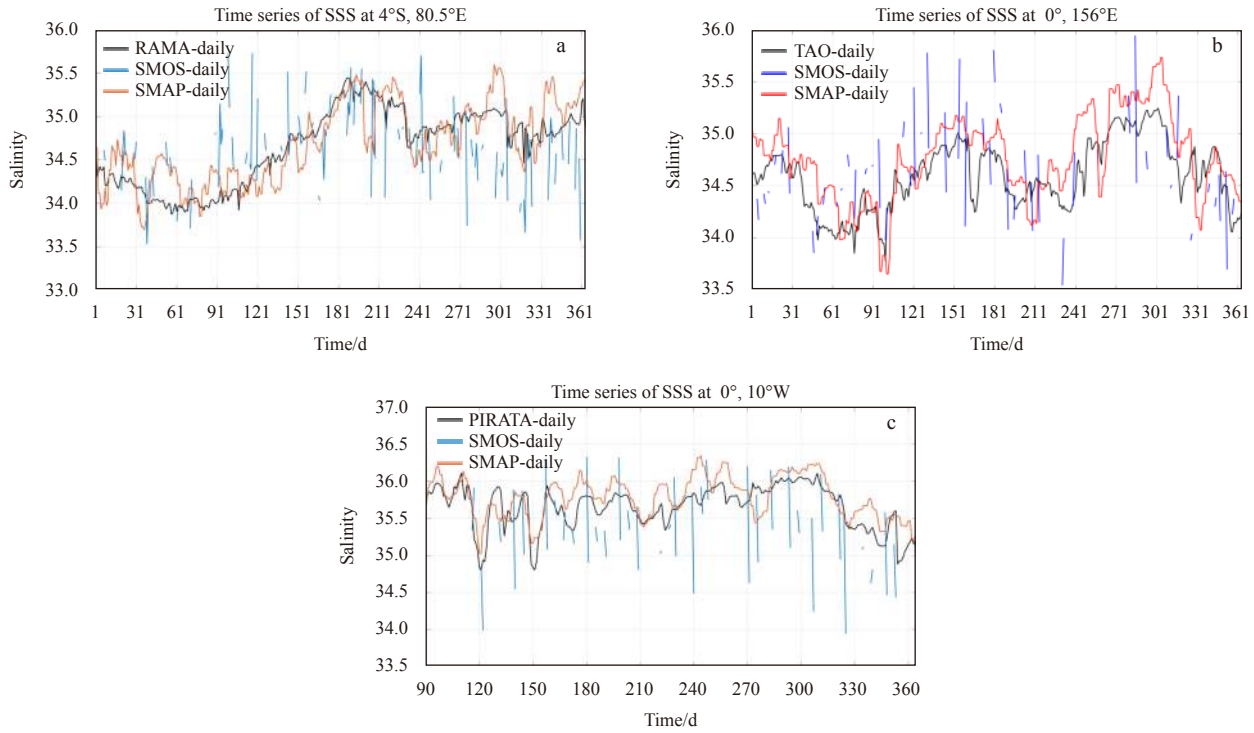

Fig. 7. Time series of the daily SMOS (blue) and daily SMAP (red) SSS products versus the moored buoys (black) at 4°S, 80.5°E (a), 0°, 156°E (b) and 0°, 10°W (c).

Table 2. Bias and RMSE between the satellite and buoy SSS at three locations

	4.0°S, 80.5°E		0°, 156°E		0°, 10°W	
	bias	RMSE	bias	RMSE	bias	RMSE
SMOS-daily	–0.06	0.54	0.05	0.46	–0.36	0.68
SMAP-daily	0.03	0.28	0.17	0.30	0.14	0.24

and the RMSE had decreased from 0.30 to 0.27, when the correction process has been applied. Therefore, it was evident that the corrected SMAP product was much closer to the TAO moored-buoy data for 2016 than the original SMAP data.

In conclusion, the applied corrections could be used to correct the daily SMAP product. As a result, the daily SMAP product was much closer to the Argo floats and moored-buoy data.

5 Discussion and conclusions

It is known that an important first step in the assimilation of satellite SSS into high-resolution forecasting models is the validation of the daily satellite SSS products. The evaluations using Argo floats data provided the basic characteristics and global distributions of the satellite SSS errors. Furthermore, evaluations using moored-buoy array measurements could potentially be used to supplement the Argo data comparison results and provide the time-series distributions of the satellite errors. The validations of the SSS errors of the daily satellite product from the SMAP, and the analysis results of the primary contributions to those SSS errors were presented in this study. In addition, based on the error analysis results, a new SMAP SSS correction method has been developed. The corrected SMAP product was then re-evaluated using Argo floats and moored-buoy data.

In summary, the daily satellite SSS products were found to be in good agreement with the Argo floats and moored-buoy array measurements. The satellite SSS errors were observed to vary in the global oceans, with larger errors along the coastal and at high latitude regions (RMSE of approximately 0.7 to 0.8), and smaller errors in the open ocean and lower latitude regions (RMSE of approximately 0.3 to 0.4). In addition, the latitude-dependent bias and RMSE of the SMAP SSS were found to be primarily influenced by precipitation (correlation coefficient of approximately 0.8) and SST (correlation coefficient of approximately –0.7), respectively. Comparison of the two daily satellite products indicated that the daily SMAP SSS product has a lower RMSE and larger bias than the daily SMOS product when compared with the Argo floats data.

Furthermore, comparisons of the two satellite products demonstrated that the low-RMSE daily SMAP product could be effectively used in assimilation systems. Since the observational products used in assimilation systems must have low biases, the daily SMAP SSS product was corrected by coefficients obtained using a regression analysis method which adopted precipitation and SST values. The validations of the corrected daily SMAP product versus the Argo floats and moored-buoy data indicated a lower RMSE and bias than the original SMAP product. In the future, this unbiased satellite SSS product will be applied into the assimilation system of high-resolution forecasting models, and other existing problems as the spatial resolution differences between the currently used models and the satellite SSS products need be further discussed.

Acknowledgements

SMAP salinity data are produced by Remote Sensing Systems and sponsored by the NASA Ocean Salinity Science Team. They are available at www.remss.com. The SMOS data is extracted from the Ocean Salinity Expertise Center (CECOS) of the CNES-IFREMER Centre Aval de Traitemenent des Donnees SMOS

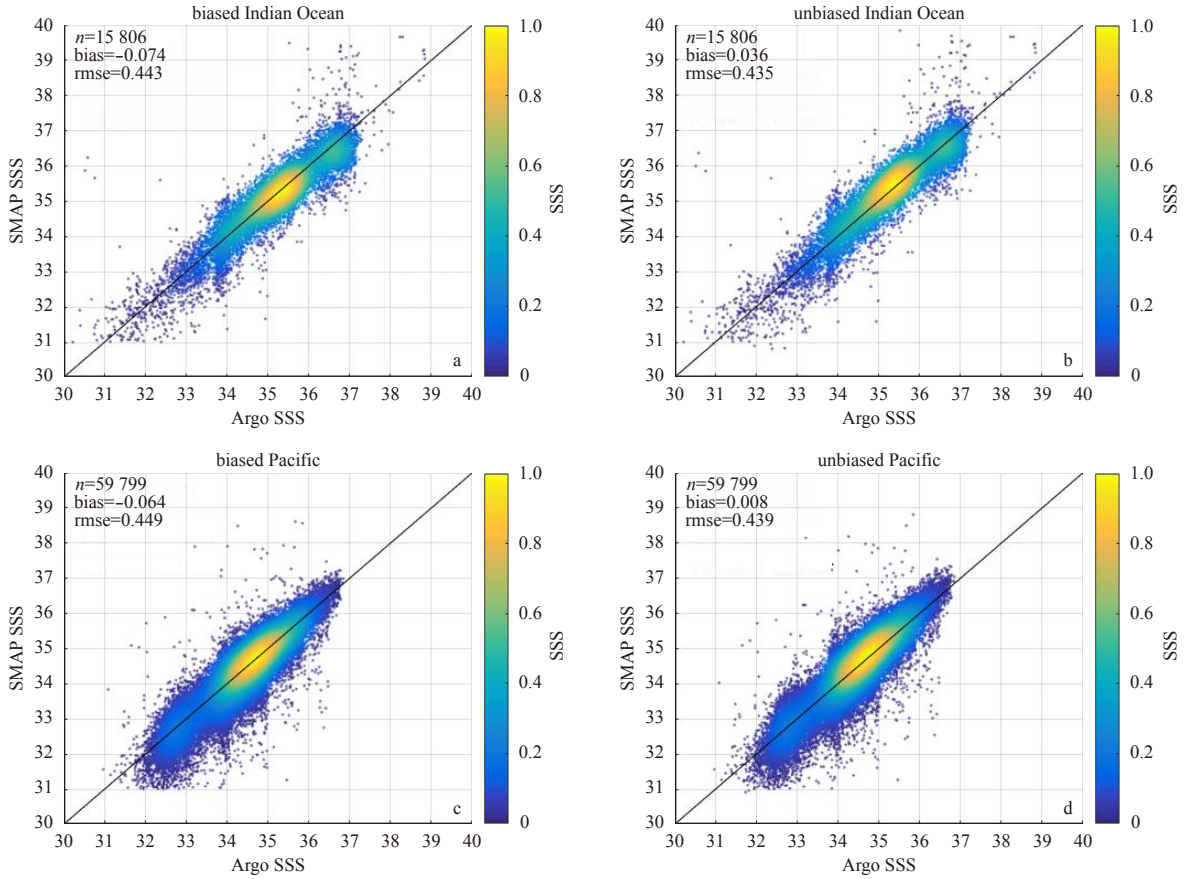

Fig. 8. Scatter plots of the SMAP SSS versus the Argo floats data in 2016. a, c. Before the bias corrections, and b, d. after the bias corrections. In this study, these were referred to as the: biased SMAP products (a, c); and unbiased SMAP products (b, d), respectively.

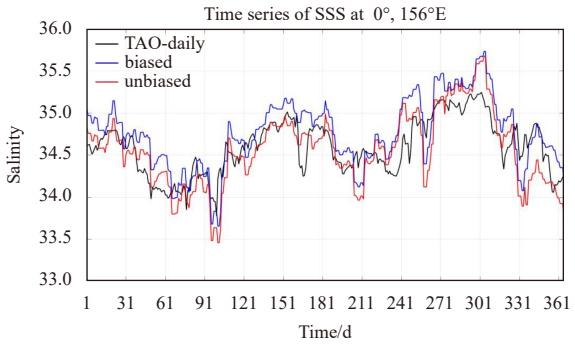

Fig. 9. Time series of the biased (blue, original SMAP product), unbiased (red, correct SMAP product), and TAO moored-buoy (black) SSS at 156°E, 0° during the year 2016

(CATDS), at IFREMER, Plouzane, France (http://www.catds.fr). Daily floats data used in this work are extracted from the Coriolis Argo Global Data Assembly Centre (ftp://ftp.ifremer.fr/ifremer/argo/). The moored buoy products are obtained from the Global Tropical Moored Buoy Array (GTMBA) office of the National Oceanic and Atmospheric Administration (NOAA) and the Pacific Marine Environmental Laboratory (PMEL). We also thank anonymous reviewers for their comments.

References

Abe H, Ebuchi N. 2014. Evaluation of sea-surface salinity observed by Aquarius. Journal of Geophysical Research: Oceans, 119(11): 8109–8121, doi: 10.1002/2014JC010094

Banks C J, Gommenginger C P, Srokosz M A, et al. 2012. Validating SMOS ocean surface salinity in the Atlantic with Argo and operational ocean model data. IEEE Transactions on Geoscience and Remote Sensing, 50(5): 1688–1702, doi: 10.1109/TGRS.2011.2167340

Berrisford P, Dee D, Poli P, et al. 2011. The ERA-interim archive: Version 2.0. Nihon Seirigaku Zasshi Journal of the Physiological Society of Japan, 31(10): 1–40

Boutin J, Martin N, Yin X B, et al. 2012. First assessment of SMOS data over open ocean: part II-sea surface salinity. IEEE Transactions on Geoscience and Remote Sensing, 50(5): 1662–1675, doi: 10.1109/TGRS.2012.2184546

Boutin J, Vergely J L, Marchand S, et al. 2018. New SMOS Sea Surface Salinity with reduced systematic errors and improved variability. Remote Sensing of Environment, 214: 115–134, doi: 10.1016/j.rse.2018.05.022

Drucker R, Riser S C. 2014. Validation of Aquarius sea surface salinity with Argo: Analysis of error due to depth of measurement and vertical salinity stratification. Journal of Geophysical Research: Oceans, 119(7): 4626–4637, doi: 10.1002/2014JC010045

Ebuchi N, Abe H. 2014. Evaluation of sea surface salinity observed by Aquarius and SMOS. In: Proceedings of 2013 IEEE International Geoscience and Remote Sensing Symposium. Melbourne: IEEE, 119: 8109–8121

Font J, Kerr Y H, Srokosz M A, et al. 2001. SMOS: a satellite mission to measure ocean surface salinity. In: Proceedings Volume 4167, Atmospheric Propagation, Adaptive Systems, and Laser Radar Technology for Remote Sensing. Barcelona: SPIE, 4167: 207–214

Garcia-Eidell C, Comiso J C, Dinnat E, et al. 2017. Satellite observed

salinity distributions at high latitudes in the northern hemisphere: a comparison of four products. Journal of Geophysical Research: Oceans, 122(9): 7717–7736, doi: 10.1002/2017JC013184

Gould J, Roemmich D, Wijffels S, et al. 2004. Argo profiling floats bring new era of in situ ocean observations. Eos Transactions American Geophysical Union, 85(19): 185–191

Hackert E, Busalacchi A J, Ballabrera-Poy J. 2014. Impact of Aquarius sea surface salinity observations on coupled forecasts for the tropical Indo-Pacific Ocean. Journal of Geophysical Research: Oceans, 119(7): 4045–4067, doi: 10.1002/2013JC009697

Kolodziejczyk N, Reverdin G, Boutin J, et al. 2015. Observation of the surface horizontal thermohaline variability at mesoscale to submesoscale in the north-eastern subtropical Atlantic Ocean. Journal of Geophysical Research: Oceans, 120(4): 2588–2600, doi: 10.1002/2014JC010455

Lagerloef G S E. 2002. Introduction to the special section: The role of surface salinity on upper ocean dynamics, air-sea interaction and climate. Journal of Geophysical Research: Oceans, 107(C12): SRF 1-1–SRF 1-2, doi: 10.1029/2002JC001669

Lagerloef G, Colomb F R, Le Vine D, et al. 2008. The Aquarius/SAC-D mission: designed to meet the salinity remote-sensing challenge. Oceanography, 21(1): 68–81, doi: 10.5670/oceanog.2008.68

Lee T. 2016. Consistency of Aquarius sea surface salinity with Argo products on various spatial and temporal scales. Geophysical Research Letters, 43(8): 3857–3864, doi: 10.1002/2016GL068822

Lu Zhengting, Cheng Lijing, Zhu Jing, et al. 2016. The complementary role of SMOS sea surface salinity observations for estimating global ocean salinity state. Journal of Geophysical Research: Oceans, 121(6): 3672–3691, doi: 10.1002/2015JC011480

Martin M J. 2016. Suitability of satellite sea surface salinity data for use in assessing and correcting ocean forecasts. Remote Sensing of Environment, 180: 305–319, doi: 10.1016/j.rse.2016.02.004

McPhaden M J. 1995. The tropical atmosphere ocean array is completed. Bulletin of the American Meteorological Society, 76(5): 739–744, doi: 10.1175/1520-0477-76.5.739

McPhaden M J, Meyers G, Ando K, et al. 2009. RAMA: the research moored array for African-Asian-Australian monsoon analysis and prediction. Bulletin of the American Meteorological Society, 90(4): 459–480, doi: 10.1175/2008BAMS2608.1

Meissner T, Wentz F J. 2016. Remote Sensing Systems SMAP Ocean Surface Salinities [Level 2C, Level 3 Running 8-day, Level 3 Monthly], Version 2.0 validated release. Remote Sensing Systems, Santa Rosa, CA, USA. www.remss.com/missions/smap

Meissner T, Wentz F J, Le Vine D M. 2018. The Salinity Retrieval Algorithms for the NASA Aquarius Version 5 and SMAP Version 3 Releases. Remote Sensing, 10(7): 1121, doi: 10.3390/rs10071121

Ratheesh S, Sharma R, Sikhakolli R, et al. 2014. Assessing sea surface salinity derived by Aquarius in the Indian Ocean. IEEE Geoscience and Remote Sensing Letters, 11(4): 719–722, doi: 10.1109/LGRS.2013.2277391

Reagan J, Boyer T, Antonov J, et al. 2014. Comparison analysis between Aquarius sea surface salinity and World Ocean Database in situ analyzed sea surface salinity. Journal of Geophysical Research: Oceans, 119(11): 8122–8140, doi: 10.1002/2014JC009961

Reul N, Tenerelli J, Chapron B, et al. 2007. Modeling sun glitter at L-band for sea surface salinity remote sensing with SMOS. IEEE Transactions on Geoscience and Remote Sensing, 45(7): 2073–2087, doi: 10.1109/TGRS.2006.890421

Servain J, Busalacchi A J, McPhaden M J, et al. 1998. A pilot research moored array in the tropical Atlantic (PIRATA). Bulletin of the American Meteorological Society, 79(10): 2019–2032, doi: 10.1175/1520-0477(1998)079<2019:APRMAI>2.0.CO;2

Tang Wenqing, Fore A, Yueh S, et al. 2017. Validating SMAP SSS with in situ measurements. Remote Sensing of Environment, 200: 326–340, doi: 10.1016/j.rse.2017.08.021

Tang Wenqing, Yueh S H, Fore A G, et al. 2014. Validation of Aquarius sea surface salinity with in situ measurements from Argo floats and moored buoys. Journal of Geophysical Research: Oceans, 119(9): 6171–6189, doi: 10.1002/2014JC010101

Terray L, Corre L, Cravatte S, et al. 2012. Near-surface salinity as nature's rain gauge to detect human influence on the tropical water cycle. Journal of Climate, 25(3): 958–977, doi: 10.1175/JCLI-D-10-05025.1

Yueh S H, Chaubell J. 2012. Sea surface salinity and wind retrieval using combined passive and active L-band microwave observations. IEEE Transactions on Geoscience and Remote Sensing, 50(4): 1022–1032, doi: 10.1109/TGRS.2011.2165075

Yueh S, Tang Wenqing, Fore A, et al. 2014. Aquarius geophysical model function and combined active passive algorithm for ocean surface salinity and wind retrieval. Journal of Geophysical Research: Oceans, 119(8): 5360–5379, doi: 10.1002/2014JC009939